EFFECTS OF HALL CURRENTS WITH HEAT AND MASS TRANSFER ON THE PERISTALTIC TRANSPORT OF A CASSON FLUID THROUGH A POROUS MEDIUM IN A VERTICAL CIRCULAR CYLINDER

by

Nabil T. M. El-DABE, Galal M. MOATIMID, Mona A. A. MOHAMED, and Yasmeen M. MOHAMED*

Department of Mathematics, Faculty of Education, Ain Shams University, Roxy, Cairo, Egypt

Original scientific paper
https://doi.org/10.2298/TSCI180222185E

In the current paper, the peristaltic transport of a non-Newtonian fluid obeying a Casson model with heat and mass transfer inside a vertical circular cylinder is studied. The considered system is affected by a strong horizontal uniform magnetic field together with the heat radiation and the Hall current. The problem is modulated mathematically by a system of PDE that describe the basic behavior of the fluid motion. The boundary value problem is analytically solved with the appropriate boundary conditions in accordance with the special case, in the absence of the Eckert number. The solutions are obtained in terms of the modified Bessel function of the first kind. Again, in the general case, the system is solved by means of the homotopy perturbation and then numerically through the Runge-Kutta Merson with a shooting technique. A comparison is done between these two methods. Therefore, the velocity, temperature and concentration distributions are obtained. A set of diagrams are plotted to illustrate the influence of the various physical parameters in the forgoing distributions. Finally, the trapping phenomenon is also discussed.

Key words: *peristaltic flow, Casson model, hall current, porous medium, heat and mass transfer*

Introduction

The mechanism of peristalsis, in both mechanical and physiological situations, has become of great importance in many scientific researches. Several theoretical and experimental attempts have been made to understand peristaltic influence in different situations. The scientists have exerted their efforts concerning the peristaltic flow of liquids. The problem of peristalsis with heat and mass transfer is analyzed by Hina *et al.* [1], chemical reaction is taken into account. Their study not only based on long wavelength and low Reynolds number approximation but also on a small Grashof number. Peristaltic flow of viscous fluid in an asymmetric inclined channel with heat transfer and the influence of an inclined magnetic field are studied by Noreen *et al.* [2]. In their work, long wavelength and low Reynolds number approximation is utilized. Peristaltic motion of a non-Newtonian nanofluid with heat transfer through a porous medium inside a vertical tube is investigated by El-Dabe *et al.* [3]. Runge-Kutta Merson method and a Newtonian iteration in a shooting and matching technique are also utilized. The influence of heat and mass transfer on the peristaltic flow of magneto hydrodynamic Eyring-Powell fluid is

* Corresponding author, yasmeenmostafa303@yahoo.com

discussed by Shaaban *et al.* [4]. Finite-difference technique is used for solving their governing system of equations. The impact of compliant walls on peristaltically induced flow of Sutterby fluid in a vertical channel is studied by Hayat *et al.* [5]. The problem formulation is based on neglecting the inertial effects and using long wavelength approximation. In their work, they observed that the velocity and temperature distributions are greater than of viscous fluid. The effects of partial slip on the peristaltic flow of a MHD Newtonian fluid are analyzed by Nadeem *et al.* [6]. The solutions of the governing system of equations are obtained by means of Adomian decomposition method. They observed that the temperature distribution decreased with the increasing of slip parameter and magnetic field parameter. Meanwhile, it increased with the increasing of the Eckert number.

The Hall effect is an ideal magnetic field sensing technology, the influence of the Hall current on a rotating unsteady flow of a conducting second grade fluid on an infinite oscillating plate is analyzed by Hayat *et al.* [7], also, the Laplace transform and the regular perturbation method are utilized to obtain the solutions of the governing equations. They observed that the boundary-layer thickness had increased with the increasing of the Hall parameter at fixed magnetic field parameter. Peristaltic transport obeying Walter's B fluid in an asymmetric channel is discussed by Mehmood *et al.* [8]. Their problem is affected by heat and mass transfer, regular perturbation method is utilized for solving their governing system of equations of motion. The peristaltic flow of an incompressible, electrically conducting Williamson fluid is investigated by Eldabe *et al.* [9]. Hall effects, viscous dissipation and Joule heating are taken into account. Peristaltic motion induced by sinusoidal traveling wave of incompressible, electrically conducting Maxwell fluid is discussed by El-Koumy *et al.* [10], Hall current with constant magnetic field is taken into account and perturbation expansion in terms of small amplitude ratio is utilized to obtain their solutions.

Casson fluids are found to be applicable in developing models for blood oxygenator. The MHD flow and heat transfer of electrically conducting viscoelastic fluids is analyzed by Akbar *et al.* [11]. Casson model is utilized to describe the viscoelastic behavior. They found that the temperature is increased with the increasing of the Casson parameter, Hartmann number, velocity slip, eccentricity parameter, thermal slip and also Brinkmann (dissipation) number. In addition, they found that the increasing in Casson parameter led to increase in the size of the trapped bolus. Casson fluid-flow over a vertical porous surface with chemical reaction in the presence of magnetic field is investigated by Arthur *et al.* [12]. Their system of PDE, which describe the problem, is solved numerically by means of the Newton-Raphson shooting method with the aid of the Fourth order Runge-Kutta algorithm. Viscous incompressible electrically conducting micropolar flow is investigated by Ali *et al.* [13]. Thermal radiation and viscous dissipation are taken into account. Quasi linearization technique is utilized to solve their coupled system of ODE. The impact of pressure stress work and thermal radiation on free convection flow around a sphere is studied by Elbashbeshy*et al.* [14]. Porous medium with Newtonian heating are taken into consideration. Finite difference technique is utilized to solve their system of non-linear PDE. Radially varying magnetic field effect on peristaltic motion obeying Jeffery model between two co-axial tubes is analyzed by Eldabe and Abou-Zeid [15]. Heat and mass transfer are taken into consideration. Their system of equations is solved analytically using regular perturbation technique.

The aim of this paper is to extend the work of Vasudev *et al.* [16] but in case of the non-Newtonian fluid which obeying Casson model [12]. The present work includes, also, the concentration equation. Hall current with heat and mass transfer are taken into account as well as viscous dissipation, chemical reaction and radiation absorption. The boundary value problem is analytically solved with the appropriate boundary conditions in accordance with the special case, in the absence of the Eckert number. The solutions are obtained in terms of the modified Bessel function of the first kind. Again, in the general case, the system is solved analytically by means of the homotopy perturbation method and numerically using Runge-Kutta Merson with the shooting technique. A comparison is done between these two methods. Therefore, the velocity, temperature and concentration distributions are obtained. A set of diagrams are plotted to illustrate the influence of the various physical parameters in the forgoing distributions. Finally, the trapping phenomenon is discussed and illustrated.

Mathematical formulation of the problem

Consider the peristaltic flow of an incompressible non-Newtonian fluid through a vertical tube. The axisymmetric cylindrical polar co-ordinate system *(R, Z)* are used, where *R*-co-ordinate is along the radial co-ordinate of the tube and *Z*-co-ordinate coincides with axis of the tube see fig. 1.

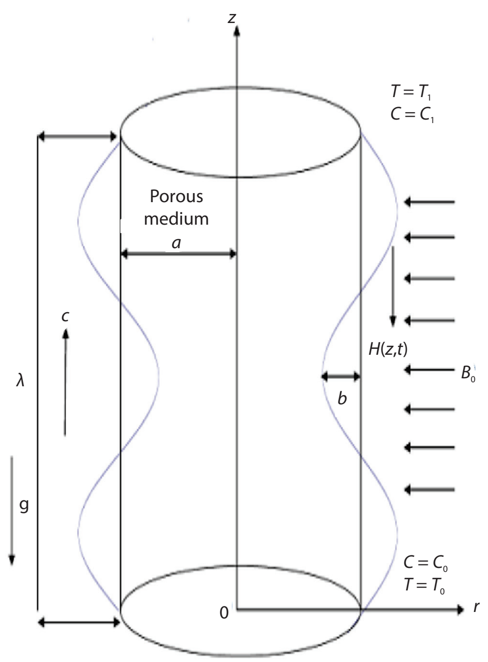

Figure 1. Physical model and co-ordinates system

The geometry of the tube wall is defined:

$$R = H(Z,t) = a + b\sin\left[\frac{2\pi(Z-ct)}{\lambda}\right] \tag{1}$$

For the unsteady 2-D flow, the velocity components, temperature and concentration may be written:

$$V = \left[U(R,Z), 0, W(R,Z)\right],\ T = T(R,Z),\ C = C(R,Z)$$

The appropriate boundary conditions are defined [16]:

$$\frac{\partial W}{\partial R} = 0,\ \ \frac{\partial T}{\partial R} = 0\ ,\ \ \frac{\partial C}{\partial R} = 0\ \ \text{at}\ R = 0 \tag{2}$$

$$W = 0,\ T = T_0,\ C = C_0\ \ \text{at}\ R = H \tag{3}$$

Introducing the following transformations between the fixed and moving frames:

$$z = Z - ct,\ r = R,\ w = W - c \tag{4}$$

The current density *J* including the Hall effect may be written [9]:

$$J = \sigma[(\underline{V}\wedge\underline{B}) - \frac{1}{en_e}(\underline{J}\wedge\underline{B})] \tag{5}$$

The governing dimensional equations of motion may be listed:

$$\frac{\partial u}{\partial r} + \frac{u}{r} + \frac{\partial w}{\partial z} = 0 \tag{6}$$

$$u\frac{\partial u}{\partial r}+w\frac{\partial u}{\partial z}=-\frac{1}{\rho}\frac{\partial P}{\partial r}+\frac{\mu_B}{\rho}\left(1+\frac{p_y}{\mu_B\sqrt{2\pi_c}}\right)\left[\frac{\partial^2 u}{\partial z^2}+2\left(\frac{\partial^2 u}{\partial r^2}+\frac{1}{r}\frac{\partial u}{\partial r}-\frac{u}{r^2}\right)\right]-$$

$$-\frac{\mu_B}{\rho K_0}u-\left[\frac{\sigma {B_0}^2}{\rho\left(1+\dfrac{\sigma {B_0}^2}{e n_e}\right)}\right]\left[u+\left(\frac{\sigma B_0}{e n_e}\right)(w+c)\right] \tag{7}$$

$$u\frac{\partial w}{\partial r}+w\frac{\partial w}{\partial z}=-\frac{1}{\rho}\frac{\partial P}{\partial z}+\frac{\mu_B}{\rho}\left(1+\frac{p_y}{\mu_B\sqrt{2\pi_c}}\right)\left[2\frac{\partial^2 w}{\partial z^2}+\frac{\partial^2 w}{\partial r^2}+\frac{1}{r}\frac{\partial w}{\partial r}+\frac{\partial^2 u}{\partial r\partial z}+\frac{1}{r}\frac{\partial u}{\partial r}\right]-$$

$$-\frac{\mu_B}{\rho K_0}(w+c)+\mathrm{g}\alpha_C(C-C_0)+\mathrm{g}\alpha_T(T-T_0)-\left[\frac{\sigma {B_0}^2}{\rho\left(1+\dfrac{\sigma {B_0}^2}{e n_e}\right)}\right]\left[w+\left(\frac{\sigma B_0}{e n_e}\right)u\right] \tag{8}$$

$$\rho c_p\left(u\frac{\partial T}{\partial r}+w\frac{\partial T}{\partial z}\right)=K\left[\frac{\partial^2 T}{\partial r^2}+\frac{1}{r}\frac{\partial T}{\partial r}+\frac{\partial^2 T}{\partial z^2}\right]+Q_0+\left(\mu_B+\frac{p_y}{\sqrt{2\pi_c}}\right)\cdot$$

$$\cdot\left[2\left(\frac{\partial u}{\partial r}\right)^2+2\left(\frac{\partial w}{\partial z}\right)^2+2\left(\frac{\partial u}{\partial r}\right)\left(\frac{\partial w}{\partial z}\right)+\left(\frac{\partial u}{\partial z}\right)^2+\left(\frac{\partial w}{\partial r}\right)^2\right]+\frac{16\sigma^* {T_0}^3}{3k^*}\left[\frac{\partial^2 T}{\partial r^2}+\frac{1}{r}\frac{\partial T}{\partial r}\right] \tag{9}$$

$$u\frac{\partial C}{\partial r}+w\frac{\partial C}{\partial z}=D\left[\frac{\partial^2 C}{\partial r^2}+\frac{1}{r}\frac{\partial C}{\partial r}+\frac{\partial^2 C}{\partial z^2}\right]-K_1(C-C_0)+\frac{DK_T}{T_m}\left[\frac{\partial^2 T}{\partial r^2}+\frac{1}{r}\frac{\partial T}{\partial r}+\frac{\partial^2 T}{\partial z^2}\right] \tag{10}$$

It is convenient to write the aforementioned eqs. (6)-(10) with the boundary conditions (2) and (3) after a transformation in an appropriate dimensionless form. This can be done in a number of ways depending primarily on the choice of the characteristic length, mass and time. Consider the following dimensionless forms:

The characteristic length, a, the characteristic mass, ρa^3, and the characteristic time, a/c. The other dimensionless quantities:

$$\begin{gathered}\bar{r}=\frac{r}{a},\ \bar{z}=\frac{z}{\lambda},\ \bar{u}=\frac{u}{c},\ \bar{w}=\frac{w}{c},\ \phi=\frac{b}{a},\ \bar{P}=\frac{Pa^2}{\mu_B},\ \Phi=\frac{C-C_0}{C_0},\ \theta=\frac{T-T_0}{T_0},\ \mathrm{Da}=\frac{K_0}{a^2}\\ \gamma=\frac{\rho a^2K_1}{\mu_B},\ \mathrm{Pr}=\frac{\mu_B c_p}{K},\ \mathrm{Re}=\frac{\rho ac}{\mu_B},\ \mathrm{Sc}=\frac{\mu_B}{\rho D},\ \mathrm{Sr}=\frac{\rho DT_0K_T}{\mu_B T_m C_0},\ \mathrm{Ec}=\frac{\mu_B c^2}{KT_0}\\ \mathrm{Gr}_C=\frac{\mathrm{g}\rho a^2\alpha_C C_0}{\mu_B c},\mathrm{Gr}_T=\frac{a^2\mathrm{g}\rho\alpha_T T_0}{\mu_B c},\ m=\frac{\sigma B_0}{en_e},\ \mathrm{M}^2=\frac{\sigma {B_0}^2a^2}{\mu_B},\ R_n=\frac{4{T_0}^3\sigma^*}{Kk^*},\ \delta=\frac{a}{\lambda}\\ \beta=\frac{\mu_B\sqrt{2\pi_c}}{p_y},\ h=\frac{H(z)}{a}=1+\phi\sin 2\pi z,\ \text{and}\ \beta_1=\frac{Q_0a^2}{KT_0}\end{gathered} \tag{11}$$

The governing equations of motion in dimensionless form after using eq. (11) and dropping the bar mark may be listed:

$$\frac{\partial u}{\partial r}+\frac{u}{r}+\frac{\partial w}{\partial z}=0 \tag{12}$$

$$\mathrm{Re}\,\delta^3\left(u\frac{\partial u}{\partial r}+w\frac{\partial u}{\partial z}\right)=-\frac{\partial P}{\partial r}-\frac{\delta^2}{\mathrm{Da}}u+\left(1+\frac{1}{\beta}\right)\cdot$$
$$\cdot\left[\delta^4\frac{\partial^2 u}{\partial z^2}+2\delta^2\left(\frac{\partial^2 u}{\partial r^2}+\frac{1}{r}\frac{\partial u}{\partial r}-\frac{u}{r^2}\right)+\delta^2\frac{\partial^2 w}{\partial r\partial z}\right]-\mathrm{M}^2\delta^2 u-\mathrm{M}^2\delta\left(w+1\right) \tag{13}$$

$$\mathrm{Re}\,\delta\left(u\frac{\partial w}{\partial r}+w\frac{\partial w}{\partial z}\right)=-\frac{\partial P}{\partial z}+\left(1+\frac{1}{\beta}\right)\left[2\delta^2\frac{\partial^2 u}{\partial z^2}+\left(\frac{\partial^2 w}{\partial r^2}+\frac{1}{r}\frac{\partial w}{\partial r}\right)+\delta^2\frac{\partial^2 u}{\partial r\partial z}+\frac{\delta^2}{r}\frac{\partial u}{\partial z}\right]-$$
$$-N^2\left(w+1\right)-\left(\frac{m\mathrm{M}^2\delta}{1+m^2}\right)u+\mathrm{Gr}_C\Phi+\mathrm{Gr}_T\theta \tag{14}$$

$$\mathrm{Re}\,\delta\,\mathrm{Pr}\left(u\frac{\partial\theta}{\partial r}+w\frac{\partial\theta}{\partial z}\right)=\left(1+\frac{4}{3}R_n\right)\left(\frac{\partial^2\theta}{\partial r^2}+\frac{1}{r}\frac{\partial\theta}{\partial r}\right)+\delta^2\frac{\partial^2\theta}{\partial z^2}+\beta_1+\mathrm{Ec}\left(1+\frac{1}{\beta}\right)\cdot$$
$$\cdot\left[2\delta^2\left(\frac{\partial u}{\partial r}\right)^2+2\delta^2\left(\frac{\partial w}{\partial z}\right)^2+2\delta\left(\frac{\partial u}{\partial z}\right)\left(\frac{\partial w}{\partial r}\right)+\delta^4\left(\frac{\partial u}{\partial z}\right)^2+\left(\frac{\partial w}{\partial r}\right)^2+2\delta^2\left(\frac{u^2}{r^2}\right)\right] \tag{15}$$

and

$$\mathrm{Re}\,\delta\,\mathrm{Sc}\left(u\frac{\partial\Phi}{\partial r}+w\frac{\partial\Phi}{\partial z}\right)=\frac{\partial^2\Phi}{\partial r^2}+\frac{1}{r}\frac{\partial\Phi}{\partial r}+\delta^2\frac{\partial^2\Phi}{\partial z^2}+$$
$$+\mathrm{ScSr}\left[\frac{\partial^2\theta}{\partial r^2}+\frac{1}{r}\frac{\partial\theta}{\partial r}+\delta^2\frac{\partial^2\theta}{\partial z^2}\right]-\gamma\mathrm{Sc}\Phi \tag{16}$$

Also, the dimensionless appropriate boundary-conditions:

$$\frac{\partial w}{\partial r}=0,\ \frac{\partial\theta}{\partial r}=0,\ \frac{\partial\Phi}{\partial r}=0\quad\text{at}\quad r=0 \tag{17}$$

$$w=-1,\ \theta=0,\ \Phi=0\quad\text{at}\quad r=h \tag{18}$$

where

$$N^2=\frac{\mathrm{M}^2}{\frac{1}{\mathrm{Da}}+\left(1+m^2\right)} \tag{19}$$

The aforementioned equations of motion are non-linear PDE. They cannot be solved in their present form. Therefore, an approximation solve these equations is considered. At this stage, under the assumptions of long wavelength approximation, $\delta \ll 1$, and low Reynolds number, $\mathrm{Re} \to 0$, these equations may be written:

$$\frac{\partial P}{\partial r}=0 \tag{20}$$

$$0=-\frac{\partial P}{\partial z}+\left(1+\frac{1}{\beta}\right)\left[\frac{1}{r}\frac{\partial}{\partial r}\left(r\frac{\partial w}{\partial r}\right)\right]-N^2\left(w+1\right)+\mathrm{Gr}_C\Phi+\mathrm{Gr}_T\theta \tag{21}$$

$$0=\left(1+\frac{4}{3}R_n\right)\left[\frac{1}{r}\frac{\partial}{\partial r}\left(r\frac{\partial\theta}{\partial r}\right)\right]+\mathrm{Ec}\left(1+\frac{1}{\beta}\right)\left(\frac{\partial w}{\partial r}\right)^2+\beta_1 \tag{22}$$

and

$$0=\left[\frac{1}{r}\frac{\partial}{\partial r}\left(r\frac{\partial\Phi}{\partial r}\right)\right]+\mathrm{ScSr}\left[\frac{1}{r}\frac{\partial}{\partial r}\left(r\frac{\partial\theta}{\partial r}\right)\right]-\gamma\mathrm{Sc}\Phi \tag{23}$$

It is worthwhile to notice that eqs. (13)-(16) are more general than these early obtained by Vasudev *et al.* [16]. In other words, on setting ($m = 0$, $\mathrm{Gr}_C = 0$, $R_n = 0$, $\mathrm{Sc} = 0$, $\mathrm{Sr} = 0$, $\mathrm{Ec} = 0$, $\beta \to \infty$, and $\gamma = 0$), one finds his previous equations (Newtonian case).

Method of solution

Solution in the special case, Ec = 0

To relax the mathematical manipulation in solving the resulted eqs. (20)-(23), the presence of the Eckert number is ignored. In this case, these equations are easily solved to yield the following solutions:

$$\theta=\frac{\beta_1 a_1}{4}\left(h^2-r^2\right) \tag{24}$$

$$\Phi=\left(\frac{\mathrm{Sr}a_1\beta_1}{\gamma}\right)\left[\frac{I_0(nr)}{I_0(nh)}-1\right] \tag{25}$$

$$\begin{aligned} w=&\frac{1}{N^2}\frac{\mathrm{d}P}{\mathrm{d}z}\left[\frac{I_0(Lr)}{I_0(Lh)}-1\right]-1+\frac{\mathrm{Gr}_T\beta_1 a_1}{4N^2}\left\{\left(h^2-r^2\right)+\frac{4}{N^2}\left(1+\frac{1}{\beta}\right)\left[\frac{I_0(Lr)}{I_0(Lh)}-1\right]\right\}+\\ &+\frac{\mathrm{Gr}_C\beta_1 a_1\mathrm{Sr}}{\gamma N^2}\left[\frac{I_0(nr)}{I_0(nh)}-1\right]\end{aligned} \tag{26}$$

where, $I_0(..)$ is the modified Bessel function of the first kind and zero order:

$$L=\sqrt{\frac{N^2\beta}{1+\beta}}\quad \text{and}\quad n=\sqrt{\gamma\mathrm{Sc}}$$

Solution in the general case, $E_c \neq 0$

Homotopy perturbation solution

In order to consider the general case, in the presence of the Eckert number, a perturbation technique may be useful. Therefore, homotopy pertubation method (HPM) is utilized. This method is considered as one of the recent perturbation methods. It can be used to solve the ordinary as well as PDE. It combines between the advantages of the homotopy analysis method (HAM) and the regular perturbation methods. The HPM is first introduced by He [17]. The HPM has been successfully applied in a different range of linear as well as non-linear differential equations by [18-21]. The method provides us, in a convenient way, an analytical or approximation solution in a wide variety for many problems arising in various fields. Away from the classical and the traditional perturbation methods, the HPM need not a small parameter or a linearization of the zero-order equation. Therefore, through this method, one can put a small parameter $p \in [0, 1]$, p is termed as the embedded homotopy parameter, as a coefficient in any term of the problem. When $p = 0$, the differential equation takes a simplified form at which it may has an analytical solution.

As p is increased and eventually takes the unity, the equation evolves the two required form. At this step, the expected solution will approach to the desired form.

The HPM is based on the initial approximation, keep in mind that this approximation must satisfy the system of the differential equations as well as the corresponding boundary--conditions. For this purpose, the following relations are defined:

$$H(p,w)=(1-p)\left[L(w)-L(w_0)\right]-p\left(\frac{1}{1+\dfrac{1}{\beta}}\right)\left[\frac{\mathrm{d}P}{\mathrm{d}z}+N^2(w+1)-\mathrm{Gr}_T\theta-\mathrm{Gr}_C\Phi\right] \tag{27}$$

$$H(p,\theta)=(1-p)\left[L(\theta)-L(\theta_0)\right]+p\left(\frac{1}{1+\dfrac{4}{3}R_n}\right)\left[\beta_1+\left(1+\frac{1}{\beta}\right)\mathrm{Ec}\left(\frac{\partial w}{\partial r}\right)^2\right] \tag{28}$$

$$H(p,\Phi)=(1-p)\left[L(\Phi)-L(\Phi_0)\right]-p\left(\frac{1}{1+A}\right)\left[\gamma\,\mathrm{Sc}\,\Phi-\mathrm{SrSc}\left(\frac{\partial^2\theta}{\partial r^2}+\frac{1}{r}\frac{\partial\theta}{\partial r}\right)\right] \tag{29}$$

with

$$L(*)=\frac{\partial^2(*)}{\partial r^2}+\frac{1}{r}\frac{\partial(*)}{\partial r}$$

is the linear operator. The initial approximation may be written:

$$w_0=-\frac{r^2}{h^2},\quad \theta_0=r^2-h^2 \quad \text{and} \quad \Phi_0=r^2-h^2 \tag{30}$$

Any of the distribution functions w, θ, and Φ may be written:

$$f(r,p)=\sum_{i=0}^{n}p^i f_i \tag{31}$$

On using the previous power series on the eqs. (27)-(29) and equating the coefficients of like powers of p on each of them and solving the resulted equations, one obtains the solutions of the different stages of p^n the procedure is lengthy but straightforward. The complete solution is obtained by setting $p = 1$. The power series up to the second-order for each of the forgoing distributions may be written:

$$w(r)=-\frac{r^2}{h^2}+(\mathrm{M}_1+\mathrm{M}_3)(r^2-h^2)-(\mathrm{M}_2+\mathrm{M}_4)(r^4-h^4)-\mathrm{M}_5(r^6-h^6) \tag{32}$$

$$\theta(r)=\left[(\mathrm{M}_6\beta_1)-1\right](h^2-r^2)+(\mathrm{M}_6\mathrm{M}_7-M_8)(h^4-r^4)+\mathrm{M}_9(h^6-r^6) \tag{33}$$

$$\Phi(r)=\frac{1}{36}\left(\frac{\gamma^2\mathrm{Sc}^2}{16}\right)(r^6-h^6)+(1-\mathrm{M}_{11})+\left[\left(\frac{-\gamma\,\mathrm{Sc}h^2}{4}\right)+\mathrm{SrSc}\right](r^2-h^2)+$$
$$+\left[\frac{\gamma\,\mathrm{Sc}}{16}+\mathrm{M}_{10}\left(\frac{\gamma^2\mathrm{Sc}^2}{16}\right)\right](r^4-h^4) \tag{34}$$

The constants a_1, M_1-M_{11} are defined but excluded here to save space.

Numerical solution

From the forgoing analysis, first the influence of the Eckert number is ignored and, secondly when this influence is considered we use the HPT. Now, the whole problem may be solved in accordance with a numerical method. On using the Runge-Kutta Merson with shooting technique, assume the following steps:

Consider the following transformations:

$$w = Y_1,\ \theta = Y_3 \text{ and } \Phi = Y_5 \tag{35}$$

Therefore, eqs. (20)-(23) may be written:

$$Y_1' = Y_2,\ Y_2' + \frac{1}{r}Y_2 = \left(\frac{1}{1+\dfrac{1}{\beta}}\right)\left[\frac{\mathrm{d}P}{\mathrm{d}z} + N^2\left(Y_1+1\right) - \mathrm{Gr}_T Y_3 - \mathrm{Gr}_C Y_5\right] \tag{36}$$

$$Y_3' = Y_4,\ Y_4' + \frac{1}{r}Y_4 = -a_1\left[\beta_1 + \left(1+\frac{1}{\beta}\right)\mathrm{Ec}\left(Y_2\right)^2\right] \tag{37}$$

$$Y_5' = Y_6,\ Y_6' + \frac{1}{r}Y_6 = \gamma\,\mathrm{Sc}Y_5 - \mathrm{SrSc}\left[Y_4' + \frac{1}{r}Y_4\right] \tag{38}$$

where the prime denotes to differentiation with respect to r.

The related boundary conditions in accordance with eqs. (36)-(38), may be written:

$$Y_1' = 0,\ Y_3' = 0 \text{ and } Y_5' = 0 \quad at \quad r = 0 \tag{39}$$

$$Y_1 = -1,\ Y_3 = 0 \text{ and } Y_5 = 0 \quad \text{at} \quad r = h \tag{40}$$

To compute the physical quantities w, θ, and Φ, MATHEMATICA package version 9 is used to solve the governing system of eqs. (36)-(38) along the appropriate boundary conditions (39) and (40). Therefore, modified Newton-Raphson iteration method continues until convergence is achieved [3] and [22].

Now, Nusselt number may be defined:

$$\mathrm{Nu} = \left(\frac{\partial\theta}{\partial r}\right)_{r=h} \tag{41}$$

Numerical discussions

In order to illustrate the quantitative effects of the different physical parameters of the problem on the distributions of the axial velocity, w, temperature, θ, and concentration, Φ, the MATHEMATICA software (package 9) is utilized. The effects of the physical parameters such as, Hall parameter, modified Grashof number, the radiation parameter, Eckert number, pressure gradien, dP/dz, Darcy number, and the non-dimensional heat source/sink parameter on these distributions are discussed numerically, graphically and illustrated through some figs. 2-4.

The variation of axial velocity, w, *vs.* the radial co-ordinate, r, for different values of R_n, modified Grashof number, Gr_C, m, Da, Ec, β_1, and dP/dz is illustrated. To make a good comparison between the HPT and the Runge-Kutta numerical technique, the following figures are characterized by the two symbols H and N to indicate the HPM and numerical calculations, respectively. The effect of the Hall parameter on the axial velocity is illustrated in fig. 2. It is observed that the velocity w decreases with the increasing of m. This is in a good agreement with the results that first obtained by Hayat *et al.* [7]. The influence of is studied, we observed that the axial velocity w increases with the increasing of Eckert number. Physically, this result are realistic, because of the magnetic field is considered as a retardant force of motion. Also, the increasing of Eckert number makes an increasing of the fluid temperature and this alternately increases the fluid-flow. To keep spaces we exclude this figure. At the same time, the numerical calculation shows that the non-dimensional Parameter, β_1, behaves like Eckert number. On the other hand, the other parameters of the problem behave like m. To avoid the repetition, we exclude these figures.

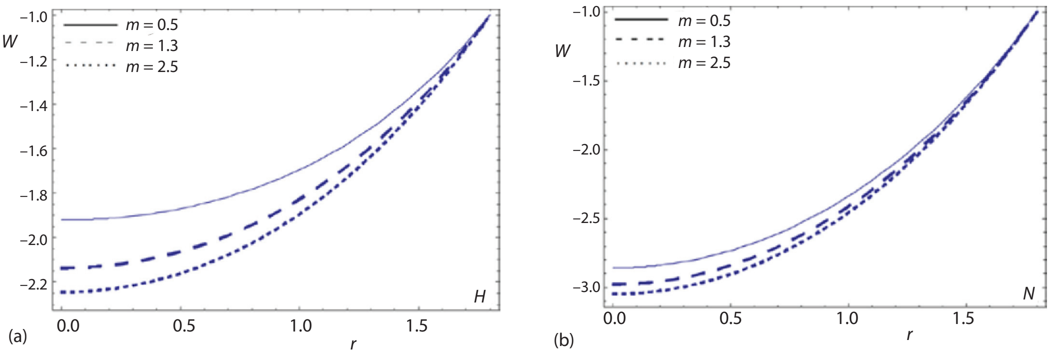

Figure 2. The axial velocity w plotted $vs.$ r under the effect of m for M = 1, Da = 0.9, Gr_T = 0.1, Ec = 3.0, Gr_C = 0.1, R_n = 0.1, dP/dz = 10, β = 0.5, β_1 = 1, Sc = 0.5, Sr = 1.0, γ = 1.5, z = 0.25, ϕ = 0.8

The variation of temperature distribution, θ, *vs.* the radial co-ordinate, r, for various values of the Eckert number, R_n, β_1, and dP/dz is illustrated. The effect of Eckert number on the temperature, θ, is graphed in fig. 3. As seen from this figure, the temperature distribution is increased with the increasing of Eckert number. The influence of R_n is also studied; we found that the temperature distribution is decreased with the increasing of R_n. To keep spaces we exclude this figure. This observation gives a good agreement with this obtained by Eldabe *et al.* [3]. As before, the numerical calculations show that the influence of the physical parameters β_1 and dP/dz, on the temperature distribution θ behave like the Eckert number.

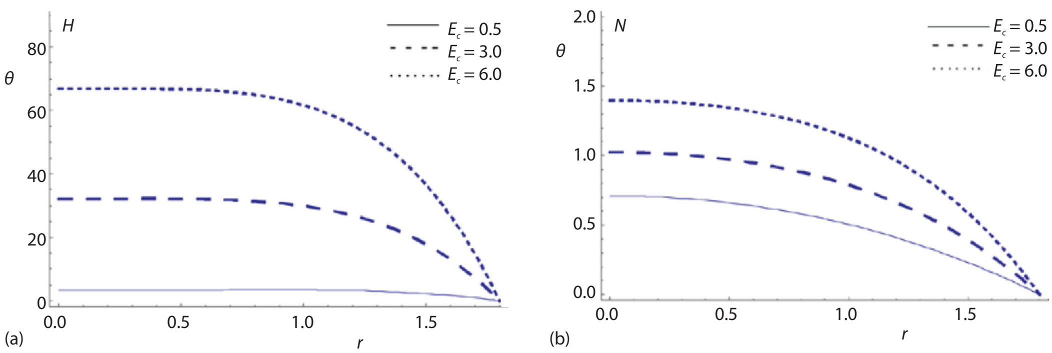

Figure 3. The temperature distribution plotted $vs.$ r under the effect of Eckert number for M = 1, Da = 0.9, Gr_T = 0.1, m = 0.5, Gr_C = 0.1, R_n = 0.1, dP/dz = 10, β = 0.5, β_1 = 1, Sc = 0.5, Sr = 1.0, γ = 1.5, z = 0.25, ϕ = 0.8

The variation of concentration distribution, Φ, *vs.* the radial co-ordinate, r, for several values of Ec, R_n, β_1, Sc, and Sr is graphed. The effect of the Schmidt number on the concentration distribution, Φ, is depicted through figs. 4. As seen from this figure, the concentration distribution, Φ, is decreased with the increasing of Schmidt number. Also, the effect of R_n on the concentration distribution, Φ, is studied; we observed that the concentration distribution, Φ, is increased with the increasing of R_n. To keep spaces we exclude this figure. This observation is in a good agreement with this obtained by Hayat *et al.* [23].

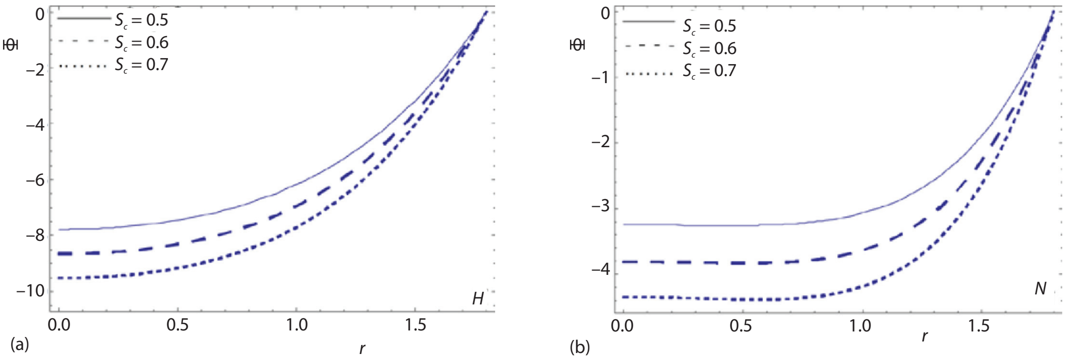

Figure 4. The concentration distribution plotted *vs.* r under the effect of Schmidt number for M = 1, Da = 0.9, Gr_T = 0.1, m = 0.5, Gr_C = 0.1, R_n = 0.1, dP/dz = 10, β = 0.5, β_1 = 1, Ec = 3.0, Sr = 1.0, γ = 1.5, z = 0.25, ϕ = 0.8

Trapping

As usual in the hydrodynamic theory, for incompressible fluids in 2-D, a stream function $\psi(r, z)$ is considered, which is defined:

$$u = \frac{1}{r}\left(\frac{\partial \psi}{\partial z}\right) \quad \text{and} \quad w = -\frac{1}{r}\left(\frac{\partial \psi}{\partial r}\right)$$

Now, the stream function $\psi(r, z)$ on the following two cases is defined as:
In the case of the absence of the Eckert number:

$$\psi(r,z) = -\left\{a_2 r\left[2I_1(Lr) - rLI_0(Lh)\right] - \frac{1}{2}r^2 + \right.$$
$$\left. + a_3 r^2\left(2h^2 - r^2\right) + a_4 r\left[2I_1(nr) - rnI_0(nh)\right]\right\} \tag{42}$$

In the case of the presence of the Eckert number:

$$\psi(r,z) = \frac{r^2}{4h^2} + (\mathrm{M}_1 + \mathrm{M}_3)\left[\frac{h^2 r^2}{2} - \frac{r^4}{4}\right] -$$
$$-(\mathrm{M}_2 + \mathrm{M}_4)\left[\frac{h^4 r^2}{2} - \frac{r^6}{6}\right] - \mathrm{M}_5\left(\frac{h^6 r^2}{2} - \frac{r^8}{8}\right) \tag{43}$$

where $I_1(..)$ is the modified Bessel function of the first kind and first order.

The constants a_2, a_3, and a_4 are defined in the appendix but excluded here to save space.

In what follows, numerical calculations with the phenomenon of trapping are made. Trapping is an important physical phenomenon in peristaltic motion. It contains a bolus of fluid with a closed streamlines. Generally, the shape of streamlines is as same as the boundary wall in the wave frame. However, under sufficient conditions, some of the streamlines split and enclose a bolus, which moves as a whole with the wave. This phenomenon is defined as trapping [24]. Figures 5 illustrated the effect of the thermal Grashof number on the streamlines. It is seen from fig. 5(a) that the size of the trapped bolus is increased with the increasing of Grashof number$_T$ in case of the absence of Eckert number. Also, the bolus size is increased with the increasing of Grashof number$_T$ in case of the presence of Eckert number which is illustrated from fig. 5(b). These results are in agreement with the results those obtained by Noreen [25]. The influence of Darcy number on the streamlines is studied; the bolus size is found to increase with the increasing of the Darcy number in case of the absence of Eckert number. Meanwhile, in case of the presence of Eckert number, the bolus size is found to decrease with the increasing of Darcy number. These results are in agreement with the results those obtained by Akbar *et al.* [26]. To keep spaces we exclude this figure. Also, the influence of the amplitude ratio, ϕ, is studied. It is observed that the bolus size is decreased with the increasing of, ϕ, in the case of absence of Eckert number. Meanwhile, in the case of presence of Eckert number the bolus size is increased with the increasing of ϕ and the bolus is disappeared at $\phi = 0$ in both cases. To avoid the repetition, we exclude these figures.

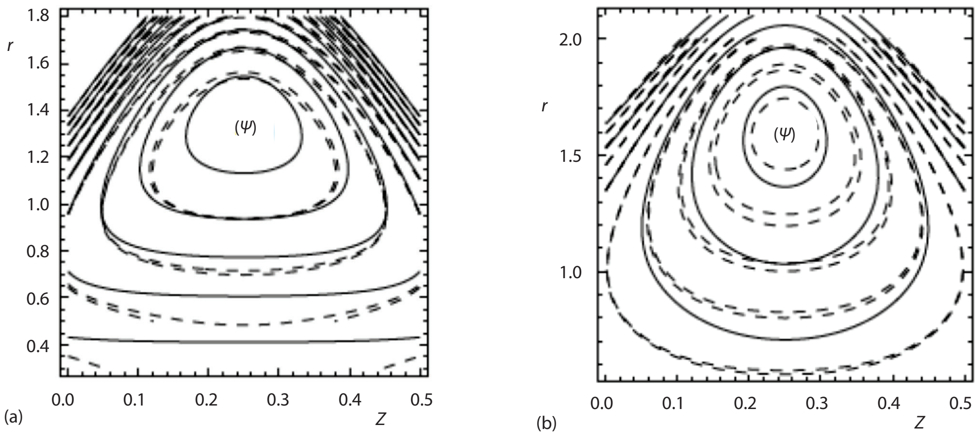

Figure 5. Streamlines for M = 1, Da = 0.9, Ec = 3.0, Gr$_C$= 0.1, R_n = 0.1, β = 0.5, β_1 = 1, Sc = 0.5, Sr = 1.0, γ = 1.5, z = 0.25, ϕ = 0.6 and for different values of Gr$_T$; Gr$_T$= 0.1, Gr$_T$= 1.5, Gr$_T$ = 1.8; (a) at Ec = 0, (b) at Ec ≠ 0

Figure 6 indicates the influence of the thermal Grashof number on the contour plot for the radial and axial velocities $u(r, z)$ and $w(r, z)$, respectively, where the radial direction, r, is plotted *vs.* the axial one z. It is observed from fig. 6(a) that the size of the trapped bolus is decreasing with the increase of Grashof number$_T$. Also, the velocity, w, is increased. Also, it is observed from fig. 6(b) the variation of velocity, w, is increased with increasing of Grashof number$_T$. Meanwhile, the size of the trapped bolus is decreasing with the increasing of Grashof number$_T$. A comparison for the temperature distribution with the work of Vasudev *et al.* [16] and the present study is illustrated in fig. 7. We found that the curves are very close at low values of R_n. A comparison of obtained results for the values of Nusselt number without effect of the Hall currents, chemical reaction parameter, Darcy, Grashof, and modified Grashof numbers with those of Eldabe [15] is illustrated through tab. 1.

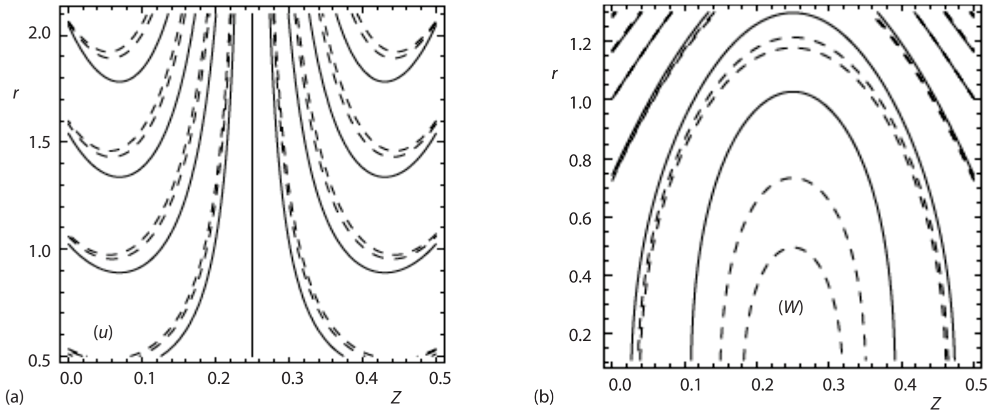

Figure 6. Contour plot for the radial and axial velocities for M = 1, Da = 0.9, Ec = 3.0, Gr_C = 0.1, R_n = 0.1, β = 0.5, β_1= 1, Sc = 0.5, Sr = 1.0, γ = 1.5, z = 0.25, ϕ = 0.6 and for different values of Gr_T; Gr_T = 0.5, Gr_T = 1.5, Gr_T = 1.8

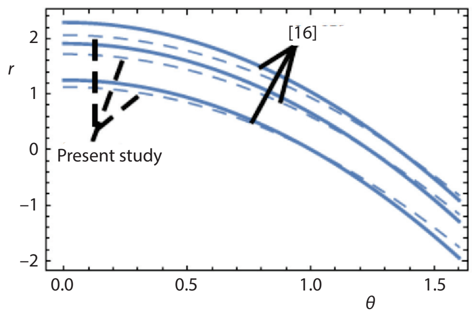

Figure 7. Comparison of temperature distribution with Vasudev work [16]

Table 1. Comparison of Nusselt number between the present results and data obtained by Eldabe and Abou-Zeid [15] for various values of Sc with R_n

R_n	Sc	M	Ec	Obtained results	Data [15]
2.5	2.5	2	5.5	–0.366222	–0.562607
3.5	3.5	2	5.5	–0.3478	–0.225751
3.5	4.5	2	5.5	–0.3316	–0.225751

Conclusions

The purpose of the current study is to investigate the effect of the Hall current on a peristaltic transport of a non-Newtonian flow. The Casson model through a vertical cylinder is taken into account. The system is affected by a strong horizontal uniform magnetic field. In addition, the heat radiation, viscous dissipation, porous media and chemical reaction are considered. The non-linear governing PDE are presented in a dimensionless form. The resulted system is very complicated to be solved analytically. To relax the mathematical manipulation, the present study depends mainly on the long wavelength approximation in addition with the law Reynolds number. The exact solution is obtained, in the absence of the Eckert number, in terms of the modified Bessel's functions of the first kind. The HPM, in the presence of the Eckert number, is utilized up to the second order. Again, a numerical technique based on the Runge-Kutta Merson with shooting technique is assumed. A set of diagrams are plotted to illustrate the influence of the various physical parameters on the velocity, temperature and concentration distributions. Also, to make a comparison between the analytical solutions and numerical ones. A graphical and data format is compared with some pervious works. A concluding comment may be drawn.

- The velocity distribution is increased in accordance with the parameters R_n, β_1, and, Ec. Meanwhile, it decreased along the parameters dP/dz, β_1, Da, Gr_T, and m. These results are in agreement with the results those obtained by Hayat *et al.* [7].
- The temperature distribution is increased in accordance with the parameters Ec and β_1. Meanwhile, it decreased along the parameters R_n and dP/dz. These results are in agreement with the results those obtained by Eldabe *et al.* [3].
- The concentration distribution is increased in accordance with the parameter R_n. Meanwhile, it decreased along the parameters Ec, Sr, β_1, and Sc. These results are in agreement with the results those obtained by Hayat *et al.* [23].

Finally, the trapping phenomenon is taken into account. The numerical calculations give the following results.

- In case of the absence of Eckert number, the influence of Darcy number is the same as the influence of Grashof number$_T$ on the bolus size.
- In case of the presence of Eckert number, the influence of Darcy number on the size of the trapped bolus is contrary to the influence of Grashof number$_T$. These results are in agreement with the results those obtained by Noreen [25] and Akbar *et al.* [26].
- Contour plots for radial and axial velocities, respectively are illustrated through figs. 6(a) and 6(b).

Nomenclature

a – initial radius of the tube
b – amplitude of the peristaltic wave
B_0 – magnetic field strength
C – concentration of the fluid
C_0 – stagnation concentration
c – wave propagation speed
c_p – specific heat parameter
D – coefficient of mass diffusivity
Da – Darcy number
Ec – Eckert number
e – electric charge
Gr_C – modified Grashof number
Gr_T – thermal Grashof number
g – gravitational acceleration
h – dimensionless of the geometry of the wall
K – thermal conductivity, [K]
K_0 – permeability of porous medium
K_1 – constant of chemical reaction
K_T – thermal diffusion ratio
k^* – mean absorption coefficient
M – Hartmann number
m – Hall parameter
n_e – number of electrons
P – fluid pressure
Pr – Prandtl number
p_y – yield stress
Q_0 – constant of heat generation
R – along the radial co-ordinate
Re – Reynolds number
R_n – radiation parameter
r – dimensionless radial co-ordinate
Sc – Schmidt number
Sr – Soret number
T_0 – stagnation temperature
T_m – mean fluid temperature
t – time
U – radial velocity of the fixed frame
u – dimensionless radial velocity
V – velocity vector
W – axial velocity of the fixed frame
w – dimensionless axial velocity
Z – axial co-ordinate
z – dimensionless axial co-ordinate

Greek symbols

α_C – coefficient of mass expansion
α_T – coefficient of thermal expansion
β – dimensionless Casson parameter
β_1 – dimensionless heat source parameter
γ – chemical reaction parameter
δ – wave number
θ – heat capacity of the fluid
λ – wave length
μ – fluid viscosity
μ_B – plastic dynamic viscosity
π – deformation rate product
π_C – critical value of deformation rate
ρ – fluid density
σ – electric conductivity
σ^* – Stefan-Boltzmann constant
τ_{ij} – stress tensor for Casson model
Φ – dimensionless concentration
ϕ – amplitude ratio
ψ – stream function

References

[1] Hina, S., *et al*., Influence of Compliant Walls on Peristaltic Motion with Heat/Mass Transfer and Chemical Reaction, *International Journal of Heat and Mass Transfer, 55* (2012), 13-14, pp. 3386-3394
[2] Noreen, S., Qasim, M., Peristaltic Flow with Inclined Magnetic Field and Convective Boundary Conditions, *Applied Bionics and Biomechanics*, *11* (2014), ID426217
[3] El-Dabe, N. T., *et al*., Magneto Hydrodynamic Peristaltic Flow of Jeffery Nanofluid with Heat Transfer through a Porous Medium in a Vertical Tube, *Applied Mathematics and Information Sciences*, *11* (2017), 4, pp. 1097-1103
[4] Shaaban, A. A., Abou-Zeid, M. Y., Effects of Heat and Mass Transfer on MHD Peristaltic Flow of a Non-Newtonian Fluid through a Porous Medium between Two Coaxial Cylinders, *Mathematical Problems in Engineering*, *2013* (2013), ID819683
[5] Hayat, T., *et al*., Peristaltic Flow of Sutterby Fluid Channel with Radiative Heat Transfer and Compliant Walls: A Numerical Study, *Results in Physics*, *6* (2016), C, pp. 805-810
[6] Nadeem, S., Akram, S., Heat Transfer in a Peristaltic Flow of MHD Fluid with Partial Slip, *Commun Non-Linear Sci Numer Simulat*, *15* (2010), 2, pp. 312-321.
[7] Hayat, T., *et al.*, Effects of Hall Current on Unsteady Flow of a Second Grade Fluid in a Rotating System, *Chemical Engineering Communications*, *192* (2005), 10, pp. 1272-1284
[8] Mehmood, O. U., *et al*., Non-Linear Peristaltic Flow of Walter's B Fluid in an Asymmetric Channel with Heat Transfer and Chemical Reactions, *Thermal Science*, *18* (2014), 4, pp. 1065-1107
[9] El-Dabe, N. T., *et al*., Hall Effects on the Peristaltic Transport of Williamson Fluid through a Porous Medium with Heat and Mass Transfer, *Applied Mathematical Modelling*, *40* (2016), 1, pp. 315-328
[10] El-Koumy, S. R., *et al*., Hall and Porous Boundaries Effects on Peristaltic Transport Through Porous Medium of a Maxwell Model, *Transport Porous Medium*, *94* (2012), 3, pp. 643-658
[11] Akbar, N. S., *et al.*, MHD Dissipative Flow and Heat Transfer of Casson Fluids due to Metachronal Wave Propulsion of Beating Cilia with Thermal and Velocity Slip Effects Under an Oblique Magnetic Field, *Acta Astronautica*, *128* (2016), Nov.-Dec., pp. 1-12
[12] Arthur, E. M., *et al*., Analysis of Casson Fluid-flow Over a Vertical Porous Surface with Chemical Reaction in the Presence of Magnetic Field, *Journal of Applied Mathematics and Physics*, *3* (2015), 6, pp. 713-723
[13] Ali, K., *et al.*, On Combined Effect of Thermal Radiation and Viscous Dissipation in Hydromagnetic Micropolar Fluid-flow Between two Stretchable Disks, *Thermal Science*, *21* (2017), 5, pp. 2155-2166
[14] Elbashbeshy, E. M. A., *et al*., Effects of Pressure Stress Work and Thermal Radiation on Free Convection Flow around a Sphere Embedded in a Porous Medium with Newtonian Heating, *Thermal Science*, *22* (2018), 1B, pp. 401-412
[15] El-Dabe, N., Abou-Zeid, M., Radially Varying Magnetic Field Effect on Peristaltic Motion with Heat and Mass Transfer of a Non-Newtonian Fluid between Two Co-Axial Tubes, *Thermal Science*, *22* (2016), 6, pp. 2449-2458
[16] Vasudev, C., *et al*., Peristaltic Flow of a Newtonian Fluid through a Porous Medium in a Vertical Tube under the Effect of a Magnetic Field, *International Journal of Current Scientific Research*, *1* (2011), 3, pp. 105-110
[17] He, J. H., Homotopy Perturbation Technique, *Computer Methods in Applied Mechanics and Engineering*, *178* (1999), 3, pp. 257-262
[18] Kumar. H., Homotopy Perturbation Method Analysis to MHD Flow of a Radiative NanoFluid with Viscous Dissipation and Ohmic Heating over a Stretching Porous Plate, *Thermal Science*, *22* (2018), 1B, pp. 413-422
[19] Rajeev, Homotopy Perturbation Method for a Stefan Problem with Variable Latent Heat, *Thermal Science*, *18* (2014), 2, pp. 391-398
[20] Abou-Zeid, M., Homotopy Perturbation Method to MHD Non-Newtonian NanoFluid-flow through a Porous Medium in Eccentric Annuli with Peristalsis, *Thermal Science*, *21* (2017), 5, pp. 2069-2080
[21] Abou-Zeid, M., Effects of Thermal-Diffusion and Viscous Dissipation on Peristaltic Flow of Micropolar Non-Newtonian Nanofluid: Application of Homotopy Perturbation Method, *Results in Physics*, *6* (2016), C, pp. 481-495
[22] Abou-Zeid, M. Y., *et al*., Numerical Treatment and Global Error Estimation of Natural Convective Effects on Gliding Motion of Bacteria on a Power-Law Nanoslime through a Non-Darcy Porous Medium, *Journal of Porous Media*, *18* (2015), 11, pp. 1091-1106

[23] Hayat, T., *et al*., Heat and Mass Transfer Effects on Peristaltic Flow of an Oldroyd-B Fluid in a Channel with Compliant Walls, *Heat Transfer-Asian Research*, *41* (2012), 1, pp. 63-83
[24] Ali, N., *et al*., Slip Effects on the Peristaltic Flow of a Third Grade Fluid in a Circular Cylindrical Tube, *Journal of Applied Mechanics*, *76* (2009), 1, pp. 1-10
[25] Noreen, S., Mixed Convection Peristaltic Flow of Third Order Nanofluid with an Induced Magnetic Field, *Plos One*, *8* (2013), 11, pp. 1-15
[26] Akbar, N. S., *et al*., NanoFluid-Flow in Tapering Stenosed Arteries with Permeable Walls, *International Journal of Thermal Science*, *85* (2014), Nov., pp. 54-61

Paper submitted: February 22, 2018
Paper revised: May 18, 2018
Paper accepted: June 4, 2018